ARTICLE

doi:10.1038/nature13724

A synaptic and circuit basis for corollary discharge in the auditory cortex

David M. Schneider[1]*, Anders Nelson[1]* & Richard Mooney[1]

Sensory regions of the brain integrate environmental cues with copies of motor-related signals important for imminent and ongoing movements. In mammals, signals propagating from the motor cortex to the auditory cortex are thought to have a critical role in normal hearing and behaviour, yet the synaptic and circuit mechanisms by which these motor-related signals influence auditory cortical activity remain poorly understood. Using *in vivo* intracellular recordings in behaving mice, we find that excitatory neurons in the auditory cortex are suppressed before and during movement, owing in part to increased activity of local parvalbumin-positive interneurons. Electrophysiology and optogenetic gain- and loss-of-function experiments reveal that motor-related changes in auditory cortical dynamics are driven by a subset of neurons in the secondary motor cortex that innervate the auditory cortex and are active during movement. These findings provide a synaptic and circuit basis for the motor-related corollary discharge hypothesized to facilitate hearing and auditory-guided behaviours.

In a wide variety of sensory systems, including the auditory system, copies of motor signals (that is, corollary discharge signals) are used to modulate sensory processing in a movement-dependent manner[1–7]. In humans, evidence of this motor influence includes modulation of auditory cortical activity during vocalization and music-related manual gestures[8–10]. More broadly, corollary discharge signals are theorized to facilitate hearing during acoustic behaviours, to convey predictive signals important for complex forms of motor learning, such as speech and music, and to drive auditory hallucinations in certain pathological states[11–15].

While motor-related signals are likely to influence auditory processing at many sites in the brain[1,11,16,17], those operating at cortical levels are apt to be especially important to learning acoustic behaviours and generating auditory hallucinations[1,11,12,17,18]. Although the synaptic and circuit origins of corollary discharge signals in the auditory cortex remain enigmatic, a direct projection from the motor cortex to the auditory cortex is a common feature of the mammalian brain[19–21], providing a substrate for conveying corollary discharge signals to the auditory cortex. Moreover, heightened motor cortical activity correlates with auditory cortical suppression in humans[22], and activating motor cortical synapses in the auditory cortex suppresses tone-evoked auditory cortical responses in the anaesthetized mouse[20].

Despite the widespread observation that movement can modulate auditory cortical activity and the presumed role of the motor cortex in driving this modulation, the synaptic and circuit mechanisms by which the motor cortex influences auditory cortical activity during movement remain unresolved. Identifying these mechanisms requires integrating high-resolution electrophysiology techniques with circuit dissection strategies in freely behaving animals to establish causal links among synapses, circuits and behaviour. Here we combine *in vivo* intracellular physiology with optogenetic circuit manipulations in freely behaving mice to identify a synaptic signature of movement in the auditory cortex and to elucidate local and long-range circuits that modulate auditory cortical activity during movement.

Movement modulates auditory cortex

To begin to study how movement modulates auditory cortical processing at synaptic and circuit levels, we used a miniature motorized microdrive to make sharp electrode intracellular current-clamp recordings from putative auditory cortical excitatory neurons of freely behaving mice (Fig. 1a, b; Extended Data Fig. 1a; cells were classified as putative excitatory cells based on their intrinsic properties, spontaneous and DC-evoked action potential patterns and, in a subset of neurons, intracellular staining and post-hoc visualization). This approach permitted intermediate to long duration recordings (mean recording duration: 14.25 min, up to 155 min) accompanied by simultaneous video monitoring of head and body movements (Extended Data Fig. 1b–d). Immediately before and during a variety of movements including locomotion, head movements, and other body movements such as grooming, auditory excitatory neurons exhibited decreased variability in their sub-threshold membrane potential fluctuations and a slight depolarization (Fig. 1c, e). We also were able to elicit vocalizations in a subset of experiments (5 neurons in 3 mice) and although vocalizations were always accompanied by other head and body movements, the membrane potential dynamics during vocalization were indistinguishable from those observed during head movements, body movements, and translocation (Extended Data Fig. 2a, b). Therefore, the sub-threshold dynamics of mouse auditory cortical excitatory cells change in a stereotyped manner before and during the execution of a wide variety of natural behaviours.

To more precisely interrogate the relative timing between movement initiation and movement-related signals in the auditory cortex and to facilitate stimulus presentation and optogenetic manipulation of neuronal activity, we developed a head-fixed preparation for recording intracellular auditory cortical activity from mice free to move or rest on a quiet, non-motorized treadmill (Fig. 1b, Extended Data Fig. 1e–i, Extended Data Fig. 2c–e). The changes in membrane potential dynamics in the auditory cortex of head-fixed mice during treadmill locomotion, grooming, facial movements, posturing and forelimb movements were indistinguishable from those we observed in unrestrained, freely behaving mice, were consistent across superficial and deeper cortical layers, and also resembled state-dependent changes that have been observed in the mouse auditory cortex[23] (Fig. 1d, e, Extended Data Fig. 2f–h). By monitoring the onset and duration of locomotor bouts, we found that changes in membrane potential dynamics of auditory cortical excitatory neurons preceded locomotion on average by >200 ms and typically outlasted locomotion by a similar

[1]Department of Neurobiology, Duke University School of Medicine, Durham, North Carolina 27710, USA.
*These authors contributed equally to this work.

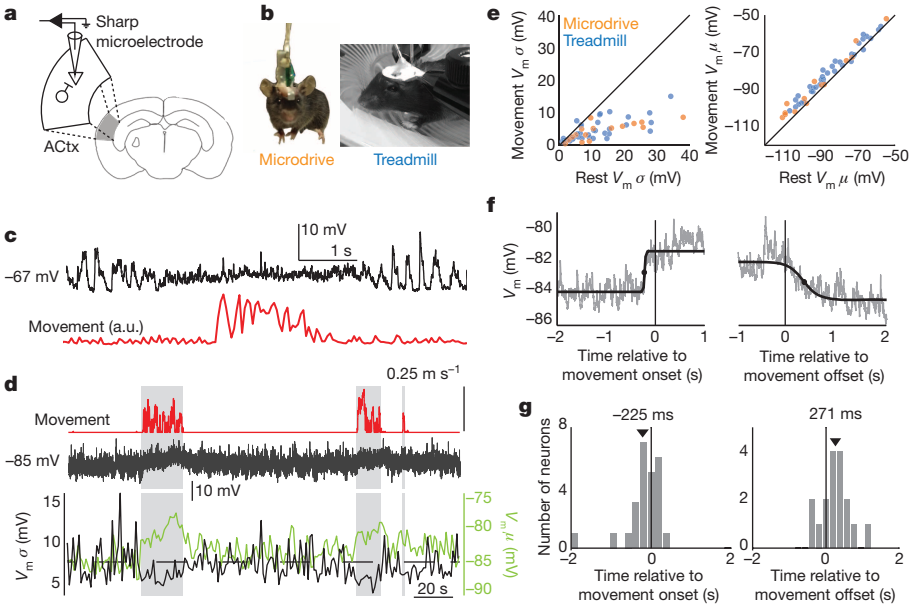

Figure 1 | Movement modulates membrane potential dynamics of auditory cortical neurons. **a**, Schematic showing sharp microelectrode current-clamp recording from an auditory cortical (ACtx) excitatory neuron in the behaving mouse. **b**, Video stills showing mouse with intracellular microdrive (left) and head-fixed mouse on treadmill (right). **c**, Membrane potential (top) of an auditory cortical neuron in an unrestrained mouse during rest and a brief movement (bottom; a.u., arbitrary units). **d**, Membrane potential (middle) of an auditory cortical neuron in a head-restrained mouse during rest and long bouts of locomotion on a treadmill (top). The bottom panel depicts the variance (σ) and mean (μ) of membrane potential (V_m) across time. **e**, Membrane potential variance and mean during rest versus movement ($n = 16/37$ cells for microdrive/treadmill, $P < 0.001$ for variance and mean, paired t-test). **f**, Membrane potential of an example neuron relative to movement onset and offset, averaged across 20 movements. Black lines show sigmoidal fit and the black dots show half rise/fall times. **g**, Histogram of the lag between membrane depolarization and movement onset (left, $P = 0.06$, t-test) and membrane hyperpolarization and movement offset (right, $P = 0.01$, t-test). Black arrows indicate population means ($n = 25$ cells). Statistical details in Methods.

duration (Fig. 1f, g). The finding that changes in auditory cortical membrane potential dynamics preceded locomotion onset by several to many hundreds of milliseconds indicates they cannot be caused by sensory reafference generated by the ensuing movements, and instead could reflect a motor-related signal. Moreover, movement-related changes in auditory cortical membrane potential dynamics persisted in the presence of broadband noise that was sufficiently loud to mask tone-evoked responses, further supporting the motor-related nature of these signals (Extended Data Fig. 3).

Suppression is local to cortex

In the visual cortex of the mouse, pyramidal neurons also display less variable and more positive membrane potentials before and during locomotion[5], and these changes are accompanied by a heightened responsiveness to visual stimuli[5,24,25]. In contrast, in the auditory cortex sound-evoked action potential responses are often suppressed during movement and during task engagement[11,23,26]. To determine whether stimulus-evoked responses in the auditory cortex of the mouse were enhanced or suppressed during movement, we presented tones at a neuron's best frequency during periods of rest and movement. In contrast to findings in the visual cortex, stimulus (that is, tone)-evoked synaptic responses of auditory cortical excitatory neurons were significantly diminished during movements (Fig. 2a, b, Extended Data Fig. 4a). Furthermore, in a small subset of neurons ($n = 4$) for which we measured tone-evoked responses during rest and movement at several different stimulus frequencies, we observed suppression during movement at all frequencies tested (Extended Data Fig. 4b).

Motor-related signals could modulate sound-evoked responses at multiple sites, spanning from the tympanic membrane to the auditory cortex[11,27], leading us to quantify the degree to which the motor-related suppression of tone-evoked responses occurs locally within the auditory cortex. We used viral vectors to express channelrhodopsin-2 (ChR2) in auditory thalamic neurons and subsequently placed an optical fibre over the auditory cortex to enable selective optical activation of thalamocortical axons (Fig. 2c, Extended Data Fig. 5a). Whereas acoustic stimulation activates the auditory system from the periphery to the cortex, this optogenetic approach allowed us to effectively bypass the ascending auditory pathway before the thalamocortical projection and to thus isolate the component of motor-related suppression that occurs within the auditory cortex. Movement was accompanied by a strong suppression of optogenetically evoked synaptic potentials recorded in auditory cortical excitatory neurons, consistent with a cortical locus (Fig. 2d, e). We also found that the degree of suppression of optogenetically evoked activity during movement was linearly related to the degree of suppression of tone-evoked activity during movement (slope = 0.6), indicating that approximately 60 per cent of the movement-related suppression of tone-evoked responses in auditory cortical excitatory neurons arises through mechanisms local to the auditory cortex (Fig. 2f).

Together, these findings indicate that motor-related signals act in the auditory cortex to suppress sensory responses in auditory cortical excitatory neurons, pointing to the engagement of local inhibition. The intracellular methods used here allowed us to measure several properties of excitatory neurons, including their intrinsic excitability, input resistance, and the reversal potential of their motor-related synaptic currents, that can be used to further determine whether this inhibition acts at a pre- or postsynaptic locus. Injecting positive and negative current pulses through the recording electrode revealed that movement was accompanied by decreased excitability and input resistance of auditory cortical excitatory neurons, and these changes also could be detected before movement onset (Fig. 2g–j, Extended Data Fig. 5b–d). Additionally, tonic current injection was used to vary the resting potential of a subset of neurons. The movement-related change in mean membrane potential reversed in sign at approximately −72 mV, which was 3 mV depolarized relative to the average resting V_m and close to the chloride equilibrium potential reported for mouse auditory cortical pyramidal neurons[28] (Extended Data Fig. 6).

All of these features indicate that motor-related signals suppress auditory cortical excitatory cells via postsynaptic inhibition, but do not exclude the possibility that presynaptic inhibition is also involved. Specifically,

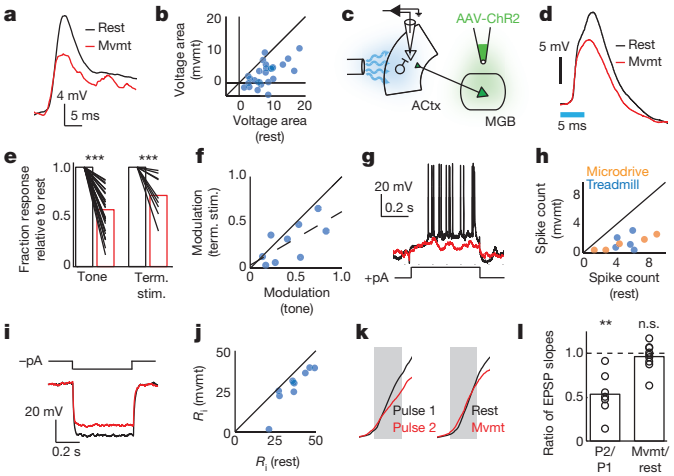

Figure 2 | Auditory cortical excitatory neurons are suppressed during movement. **a**, An example neuron's response to a preferred tone during rest (black) and movement (mvmt; red). **b**, The voltage area response of multiple neurons to preferred tone stimulus during rest versus movement ($n = 27$, $P < 0.001$, paired t-test). **c**, Schematic showing viral infection of AAV-ChR2 into medial geniculate body (MGB) and optogenetic activation of ChR2$^+$ axon terminals in the auditory cortex. **d**, Responses of an example neuron to optogenetic stimulation of thalamocortical terminals during rest (black) and movement (red). Blue bar indicates duration of light stimulation. **e**, Normalized responses to preferred tone stimulus (left, $n = 27$, t-test) and thalamocortical terminal stimulation (term. stim.; right, $n = 9$, t-test) during rest (black bars) and movement (red bars). **f**, Modulation of tone-evoked versus thalamocortical terminal stimulation. Modulation was defined as $(1 - R_{mvmt}/R_{rest})$, where R_{mvmt} and R_{rest} were the peak response during movement and rest, respectively. Dashed line shows the linear regression ($n = 9$, $r = 0.69$). **g**, Evoked response of an example neuron to intracellular positive current injection during rest (black) and movement (red). **h**, Number of spikes evoked by positive current injection during rest versus movement ($n = 5/5$ for microdrive/treadmill, $P < 0.001$, paired t-test). **i**, Evoked voltage response of an example neuron to intracellular negative current injection during rest (black) and movement (red). **j**, Input resistance (R_i) during rest versus movement ($n = 10$, $P < 0.001$, paired t-test). **k**, Initial phase of the EPSP evoked by optogenetic stimulation of thalamic terminals in the auditory cortex. Left panel shows the responses to two sequential pulses delivered 50 ms apart. Right panel shows the responses to pulses delivered during rest and movement. **l**, Ratio of the EPSP slopes measured during paired-pulse stimulation (pulse 2 vs pulse 1, P2/P1; $n = 7$, t-test) and during movement vs rest ($n = 9$, t-test). n.s., not significant; $^{**}P < 0.01$, $^{***}P < 0.001$. Statistical details in Methods.

task-engagement has been shown to augment auditory thalamic neuron activity[29,30], which could depress thalamic terminals in the auditory cortex. To explore this possibility we first established that optogenetically stimulating auditory thalamocortical synapses at >20 Hz was sufficient to decrease the onset slope of the evoked excitatory postsynaptic potential (EPSP), which provides a postsynaptic readout of presynaptic depression (Fig. 2k, l)[31,32]. We then measured the onset slope of optogenetically evoked thalamocortical synaptic potentials, and found no difference in the rising slope of the EPSP across movement and rest conditions, indicating that thalamic terminals in the auditory cortex are not depressed during movement (Fig. 2k, l). Therefore, motor-related suppression of tone-evoked responses in the auditory cortex involves postsynaptic inhibition on excitatory neurons.

PV$^+$ neurons are active during movement

To explicitly test if auditory cortical inhibitory neurons were recruited by a motor-related signal and involved in movement-related changes in excitatory neuron activity, we monitored the spiking activity of a large population of neurons using a multi-electrode array inserted across a broad expanse of the auditory cortex in mice engineered to express ChR2

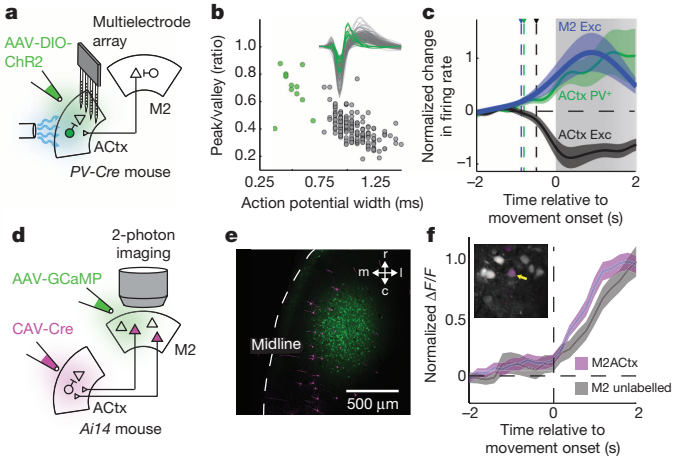

Figure 3 | Auditory cortical PV$^+$ interneurons and M2$_{ACtx}$ neurons are active during movement. **a**, Schematic showing viral infection of PV-Cre mice with a Cre-dependent ChR2 construct. **b**, Width and peak-to-valley ratio of action potentials of excitatory (black, $n = 173$) and PV$^+$ (green, $n = 12$) auditory cortical neurons. Inset shows average action potential of every neuron. **c**, Average spiking activity of excitatory (black) and PV$^+$ (green) populations in the auditory cortex and excitatory M2 neurons (blue, $n = 90$) relative to movement onset, normalized to spontaneous firing levels during rest. Triangles and dashed vertical lines show time of significant deviation from resting. All movements lasted at least 1 s, and 80 per cent of movements persisted for at least 2 s, as indicated by gradation of grey bar. **d**, Schematic showing Cre-dependent expression of tdTomato in M2$_{ACtx}$ neurons, injection of M2 with GCaMP6s, and two-photon calcium imaging. **e**, tdTomato$^+$ and tdTomato$^-$ M2 neurons expressing GCaMP6s in M2 *ex vivo*. **f**, Change in fluorescence of tdTomato$^+$ ($n = 7$) and tdTomato$^-$ ($n = 23$) M2 neurons aligned to movement onset. Inset shows a representative imaging region in M2 with tdTomato$^+$ and tdTomato$^-$ M2 neurons expressing GCaMP6s. Data show mean ± s.e. Statistical details in Methods.

in parvalbumin-positive (PV$^+$) or other GABAergic neurons (Fig. 3a, Extended Data Fig. 7a, b, PV–ChR2 and vesicular GABA transporter (VGAT)–ChR2 mice, respectively)[33]. We then classified neurons as PV$^+$ cells, inhibitory cells or excitatory cells on the basis of their action potential shapes (Fig. 3b, Extended Data Fig. 7c) and whether they were excited or suppressed by blue light. Before and during movements, the firing rates of PV$^+$ cells and other fast-spiking interneurons increased, whereas the firing rates of putative excitatory neurons decreased (Fig. 3c, Extended Data Fig. 7d, e). As a population, inhibitory neuron firing rates increased well before movement onset and also before the firing rates of auditory cortical excitatory cells decreased below their baseline levels (−805 ms for PV$^+$ cells, −605 ms for VGAT$^+$ cells, and −490 ms for excitatory cells, relative to movement onset). These experiments indicate that in the auditory cortex, motor-related signals excite PV$^+$ interneurons, which in turn postsynaptically inhibit excitatory cells to suppress their spontaneous activity and stimulus-evoked responses.

M2$_{ACtx}$ neurons are active during movement

What is the source of motor-related signals in the auditory cortex? Anatomical tracing studies in the mouse show that the auditory cortex receives input from several motor-related regions, including the cingulate cortex, primary motor cortex, and secondary motor cortex (M2), the last of which when optogenetically activated can drive strong feedforward inhibition in the auditory cortex mediated in part by PV$^+$ interneurons[20] (Extended Data Fig. 8a). Moreover, a subset of M2 neurons have branching axons that innervate the auditory cortex and the brainstem, providing an anatomical substrate for conveying motor-related signals to the auditory cortex[20]. If M2 is a source of motor-related signals in freely behaving mice, M2 excitatory cells should increase their firing rate before movement-related changes in auditory cortical activity. Using an extracellular array that spanned a large region of M2 in mice freely behaving

on a treadmill, we determined that M2 excitatory neuron action potential activity increased before a variety of movements, including locomotion (Fig. 3c; −870 ms, relative to movement onset). Notably, pre-movement increases in M2 activity also preceded changes in auditory cortical spiking activity and membrane potential dynamics and, at movement offset, M2 activity declined to baseline levels with a time course similar to movement offset-related changes in the auditory cortex (Extended Data Fig. 8b, c; also see Fig. 1g).

A remaining issue is whether M2 neurons that extend axons to the auditory cortex (that is, $M2_{ACtx}$ cells) display movement-related dynamics similar to the general population of M2 cells recorded here using a multi-electrode array. To resolve this issue, we used an intersectional strategy to selectively express a red fluorescent reporter in $M2_{ACtx}$ cells and then used viral methods to express the genetically encoded calcium indicator GCaMP6s[34] in broad fields of M2 neurons (Fig. 3d, e). Two-photon calcium imaging of GCaMP6s-expressing M2 neurons in head-fixed mice running on a treadmill revealed that $M2_{ACtx}$ cells exhibited movement-related increases in fluorescence with a time course indistinguishable from that of the general M2 population (Fig. 3f). Thus, $M2_{ACtx}$ cells are a source of motor-related signals that could be transmitted to the auditory cortex.

$M2_{ACtx}$ terminals drive movement-like dynamics

To begin to test whether $M2_{ACtx}$ cells can account for changes in auditory cortical dynamics like those observed during movement, we assessed whether activating M2 terminals in the auditory cortex of resting mice was sufficient to induce movement-like membrane potential dynamics in auditory cortical excitatory neurons. Following viral infection of AAV-ChR2 in M2 (Extended Data Fig. 8d), optically activating $ChR2^+$ M2 terminals in the auditory cortex of resting mice decreased the membrane potential variability and tone-evoked responses of excitatory cells, and also resulted in a slight depolarization, highly similar to the effects of movement (Fig. 4a, b, e–g). One potential concern is that optogenetic activation of M2 terminals in the auditory cortex triggers antidromic propagation of action potentials and thus excites other targets of $M2_{ACtx}$ cells, some of which may also innervate the auditory cortex. Two observations argue against such an indirect mechanism. First, optogenetic activation of M2 terminals was equally efficacious in modulating auditory cortical dynamics when M2 cell bodies were pharmacologically silenced with the sodium channel blocker tetrodotoxin (TTX; Fig. 4c–g). Second, the onset of changes in auditory cortical dynamics following optogenetic activation of M2 terminals occurred more rapidly (<7 ms) than the antidromic propagation time from auditory cortex to M2 (~12 ms) (Fig. 4h). Therefore, activating M2 terminals within the auditory cortex is sufficient to induce movement-like auditory cortical dynamics without concomitant recruitment of indirect pathways.

M2 is necessary for motor-related dynamics

These experiments raise the possibility that ongoing M2 activity is necessary for maintaining movement-related synaptic dynamics in the auditory cortex. To test this idea, we unilaterally and selectively silenced M2 excitatory neuron cell bodies during locomotion by optogenetically activating M2 inhibitory neurons in VGAT–ChR2 mice (Fig. 5a–c, Extended Data Fig. 8e). Silencing either ipsilateral or contralateral M2 (relative to the auditory cortical recording site) was sufficient to arrest movements ~500 ms after light onset (Fig. 5d–f). Notably, silencing ipsilateral M2 rapidly (~70 ms after laser onset) restored rest-like membrane potential dynamics in the auditory cortex (Fig. 5f–h), and this reversion to a rest-like state always preceded movement offset (Fig. 5f, Extended Data Fig. 8f). In contrast, silencing contralateral M2 did not lead to changes in auditory cortical excitatory neurons until after movement offset, effectively recapitulating the time course observed after spontaneous movement cessation (Fig. 5f, also see Fig. 1g, h). These differential effects of silencing ipsilateral versus contralateral M2 on auditory cortical dynamics are consistent with a previous anatomical finding that the projection from M2 to auditory cortex is almost completely ipsilateral[20].

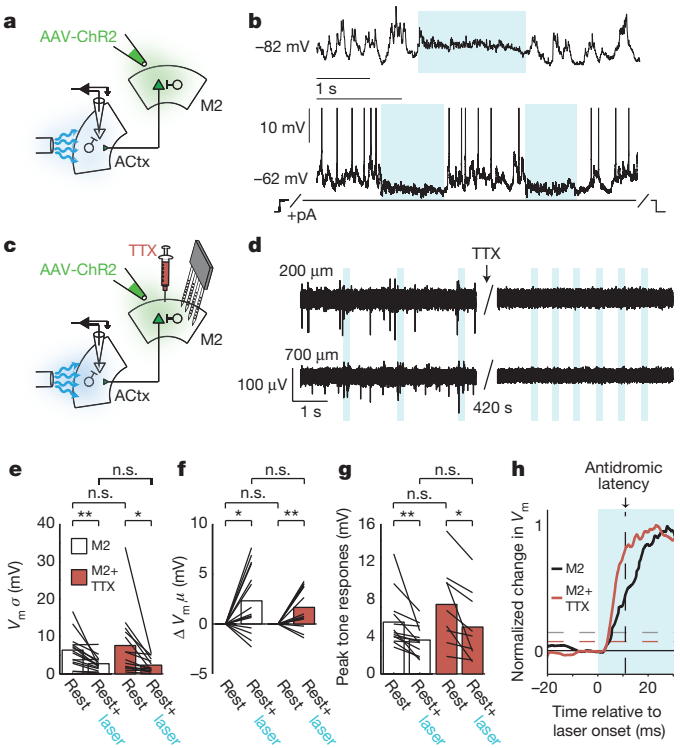

Figure 4 | M2 axon terminals in the auditory cortex are sufficient to produce movement-like auditory cortical dynamics during rest. **a**, Schematic showing intracellular recording in the auditory cortex during optogenetic activation of $ChR2^+$ M2 terminals. **b**, Optogenetic stimulation of M2 terminals in the auditory cortex causes a slight depolarization and decreased variability (top), and during tonic depolarization, M2 terminal stimulation suppresses spontaneous spiking and hyperpolarizes neurons (bottom, spikes truncated). **c**, Schematic showing intracellular recording in auditory cortex during optogenetic activation of $ChR2^+$ M2 terminals and multi-electrode array recordings in M2 during pharmacological silencing of M2 cell bodies with the sodium channel blocker, TTX. **d**, Left panels show superficial and deep recordings in M2 with spontaneous spikes (top and bottom) and antidromic spikes evoked by optogenetic stimulation of $M2_{ACtx}$ terminals (blue). Right panels show the abolition of spontaneous and antidromic spiking in M2 after TTX application. **e**–**g**, M2 terminal stimulation leads to decreases in membrane potential variability (**e**, $n = 15/14$, paired t-test), a slight depolarization (**f**, $n = 15/14$, t-test), and decreased tone-evoked responses (**g**, $n = 13/9$, paired t-test), with and without M2 cell bodies inactivated with TTX (n = number of cells recorded without/with TTX; legend in **e** applies to **e**–**g**). **h**, Normalized average change in membrane potential after M2 terminal stimulation with (red, $n = 15$) and without (black, $n = 14$) M2 cell bodies inactivated. Vertical black dashed line shows the latency of an antidromic spike travelling from the auditory cortex to M2. Horizontal dashed lines indicate significant depolarizations relative to baseline. $^*P < 0.05$, $^{**}P < 0.01$. Statistical details in Methods.

The observation that silencing the ipsilateral M2 could restore rest-like auditory cortical dynamics several hundred milliseconds before movement offset allowed us to determine whether unilaterally silencing M2 was sufficient to enhance tone-evoked responses in the ipsilateral auditory cortex while the mouse was still moving. Presenting tones during the initial phase of M2 suppression, when auditory cortical membrane potential dynamics had transitioned to a rest-like state but before locomotion offset, revealed a strong (~40 per cent) recovery of tone-evoked responses (Fig. 5i, j). We also noted that silencing M2 excitatory cell bodies in the resting mouse could slightly enhance tone-evoked responses in the auditory cortex, consistent with the idea that spontaneous activity in M2 of resting, awake mice exerts a weak suppressive effect on auditory cortical responsiveness (Fig. 5i, j). Together, these experiments dissociate the motor-related modulations we observe in the auditory cortex from movement, and show that activity in ipsilateral M2 plays a critical role

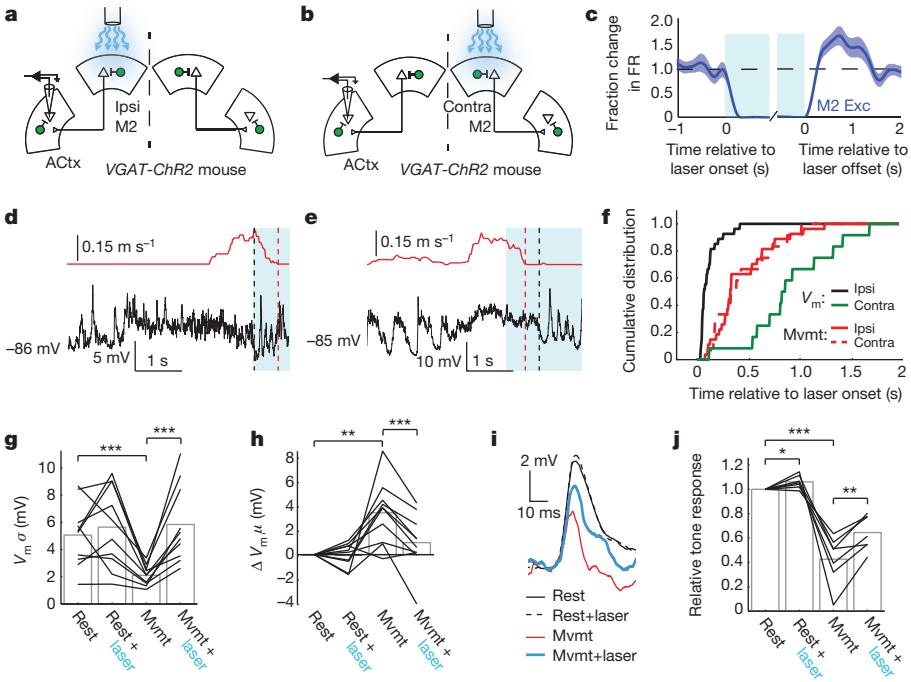

Figure 5 | M2 activity is necessary to sustain movement-related dynamics in the auditory cortex. **a**, **b**, Schematics showing intracellular recording in auditory cortex while silencing ipsilateral (**a**) or contralateral (**b**) M2. **c**, Average spiking activity (mean ± s.e.) of a population of M2 excitatory neurons ($n = 66$) before, during and after optogenetic activation of M2 inhibitory neurons (FR, firing rate). **d**, Membrane potential dynamics of example auditory cortical excitatory neuron during rest, during movement (red trace) and during movement with optogenetic suppression of ipsilateral M2 excitatory neurons (blue bar). **e**, As in **d**, but while silencing contralateral M2. **f**, Transition to rest-like membrane potential dynamics precedes movement offset with ipsilateral M2 silencing ($n = 27$, $P < 0.001$, two-sample Kolmogorov–Smirnov (KS) test) but follows movement offset with contralateral M2 silencing ($n = 12$, $P < 0.05$, two-sample KS test). **g**, **h**, Membrane potential variance (**g**, $n = 10$, paired t-test) and mean (**h**, $n = 10$, paired t-test) of auditory cortical excitatory neurons during rest and movement with and without optogenetic suppression of ipsilateral M2. **i**, Tone-evoked responses of an example neuron during rest and movement, with and without optogenetic suppression of ipsilateral M2. **j**, Tone-evoked responses of auditory cortical excitatory neurons during rest and movement, with and without optogenetic suppression of ipsilateral M2 ($n = 7$, paired t-test). $^*P < 0.05$, $^{**}P < 0.01$, $^{***}P < 0.001$. Statistical details in Methods.

in driving movement-like synaptic dynamics and controlling the gain of sensory-evoked responses in the auditory cortex.

Discussion

Projections from motor cortex to the auditory cortex are an architectural feature common to many mammalian species[19–21,35,36], including humans and other primates, and are thought to convey information critical for learning and executing complex behaviours, including speech and musicianship. Although movement-related modulation of auditory cortical activity has been detected in monkey and human auditory cortex during a variety of behaviours[1,10,11,18,37], a direct role for the motor cortex in these modulatory processes was untested. By applying a wide range of electrophysiological, optical, optogenetic and pharmacological methods in the freely behaving mouse, this study identifies a postsynaptic inhibitory signature of motor action within auditory cortex, a local source of this inhibition, and a long-range motor-to-auditory cortical circuit that engages this local inhibitory mechanism to suppress tone-evoked responses during movement. We found that a wide variety of natural movements strongly suppresses the spontaneous and tone-evoked synaptic activity of auditory cortical excitatory cells and that a substantial fraction of this suppression is mediated through a postsynaptic mechanism involving increased local inhibition via PV^+ interneurons. This mechanism contrasts with a disinhibitory mechanism implicated in locomotion-dependent increases in visual cortical responses[38], with a parallel negative rescaling of excitatory and inhibitory synaptic drive that has been advanced to account for state-dependent changes in auditory cortical responsiveness[23], and with presynaptic depression driven by state-dependent increases in thalamic activity[30]. Moreover, our observation that this suppression precedes movement onset and persists in masking noise strongly implicates a motor-related signal, rather than sensory reafference or attentional mechanisms[26]. Finally, the finding that movement can suppress ChR2-evoked auditory thalamocortical responses indicates that motor-related suppression of tone-evoked responses is not simply a consequence of peripheral masking by movement-related noise[27,39].

The present findings establish that direct ipsilateral projections from M2 to the auditory cortex are sufficient to account for movement-related auditory cortical dynamics and that activity in the ipsilateral M2 is also necessary to sustain these dynamics during movement. However, M2 and the auditory cortex are embedded in complex networks, a consequence of which is that, in addition to directly influencing auditory cortical processing, M2 could also act indirectly through or in concert with neuromodulatory cell groups[40] to modulate auditory cortical dynamics. These findings add to a growing body of evidence that motor-related signals, including those arising from motor cortical regions, can strongly modulate the stimulus-evoked responsiveness of sensory cortical neurons[1,2,4,5,24,25]. Notably, whereas the gain of stimulus-evoked responses in visual cortical pyramidal cells increases with locomotion[5,25], perhaps to compensate for increased visual flow, auditory cortical responses to tones decreased during movement. This suppressive effect, which resembles corollary discharge signals described in the auditory systems of animals ranging from insects to humans[6,41], may reflect a general strategy where motor-related signals transiently dampen sensitivity to predictable low-intensity sounds, enabling auditory neurons to maintain responsiveness to unexpected high-intensity stimuli[23,42]. Finally, motor–auditory cortical circuitry is implicated in various forms of abnormal hearing, including tinnitus[43] and auditory hallucinations[12,44], motivating future studies to investigate structural and functional changes in this circuitry in appropriate animal models.

Online Content Methods, along with any additional Extended Data display items and Source Data, are available in the online version of the paper; references unique to these sections appear only in the online paper.

Received 18 March; accepted 31 July 2014.
Published online 27 August 2014.

1. Eliades, S. J. & Wang, X. Sensory-motor interaction in the primate auditory cortex during self-initiated vocalizations. *J. Neurophysiol.* **89,** 2194–2207 (2003).
2. Lee, S., Kruglikov, I., Huang, Z. J., Fishell, G. & Rudy, B. A disinhibitory circuit mediates motor integration in the somatosensory cortex. *Nature Neurosci.* **16,** 1662–1670 (2013).
3. Maimon, G., Straw, A. D. & Dickinson, M. H. Active flight increases the gain of visual motion processing in *Drosophila*. *Nature Neurosci.* **13,** 393–399 (2010).
4. Petreanu, L. *et al.* Activity in motor-sensory projections reveals distributed coding in somatosensation. *Nature* **489,** 299–303 (2012).
5. Polack, P. O., Friedman, J. & Golshani, P. Cellular mechanisms of brain state-dependent gain modulation in visual cortex. *Nature Neurosci.* **16,** 1331–1339 (2013).
6. Poulet, J. F. & Hedwig, B. The cellular basis of a corollary discharge. *Science* **311,** 518–522 (2006).
7. Sommer, M. A. & Wurtz, R. H. A pathway in primate brain for internal monitoring of movements. *Science* **296,** 1480–1482 (2002).
8. Flinker, A. *et al.* Single-trial speech suppression of auditory cortex activity in humans. *J. Neurosci.* **30,** 16643–16650 (2010).
9. Reznik, D., Henkin, Y., Schadel, N. & Mukamel, R. Lateralized enhancement of auditory cortex activity and increased sensitivity to self-generated sounds. *Nature Commun.* **5,** 4059 (2014).
10. Zatorre, R. J., Chen, J. L. & Penhune, V. B. When the brain plays music: auditory-motor interactions in music perception and production. *Nature Rev. Neurosci.* **8,** 547–558 (2007).
11. Eliades, S. J. & Wang, X. Neural substrates of vocalization feedback monitoring in primate auditory cortex. *Nature* **453,** 1102–1106 (2008).
12. Ford, J. M. & Mathalon, D. H. Corollary discharge dysfunction in schizophrenia: can it explain auditory hallucinations? *Int. J. Psychophysiol.* **58,** 179–189 (2005).
13. Hickok, G., Houde, J. & Rong, F. Sensorimotor integration in speech processing: computational basis and neural organization. *Neuron* **69,** 407–422 (2011).
14. Houde, J. F. & Jordan, M. I. Sensorimotor adaptation in speech production. *Science* **279,** 1213–1216 (1998).
15. Paus, T., Perry, D. W., Zatorre, R. J., Worsley, K. J. & Evans, A. C. Modulation of cerebral blood flow in the human auditory cortex during speech: role of motor-to-sensory discharges. *Eur. J. Neurosci.* **8,** 2236–2246 (1996).
16. Mukerji, S., Windsor, A. M. & Lee, D. J. Auditory brainstem circuits that mediate the middle ear muscle reflex. *Trends Amplif.* **14,** 170–191 (2010).
17. Schuller, G. Vocalization influences auditory processing in collicular neurons of the CF-FM-bat, *Rhinolophus ferrumequinum*. *J. Comp. Physiol.* **132,** 39–46 (1979).
18. Curio, G., Neuloh, G., Numminen, J., Jousmaki, V. & Hari, R. Speaking modifies voice-evoked activity in the human auditory cortex. *Hum. Brain Mapp.* **9,** 183–191 (2000).
19. Budinger, E. & Scheich, H. Anatomical connections suitable for the direct processing of neuronal information of different modalities via the rodent primary auditory cortex. *Hear. Res.* **258,** 16–27 (2009).
20. Nelson, A. *et al.* A circuit for motor cortical modulation of auditory cortical activity. *J. Neurosci.* **33,** 14342–14353 (2013).
21. Reep, R. L., Corwin, J. V., Hashimoto, A. & Watson, R. T. Efferent connections of the rostral portion of medial agranular cortex in rats. *Brain Res. Bull.* **19,** 203–221 (1987).
22. Ford, J. M. & Mathalon, D. H. Electrophysiological evidence of corollary discharge dysfunction in schizophrenia during talking and thinking. *J. Psychiatr. Res.* **38,** 37–46 (2004).
23. Zhou, M. *et al.* Scaling down of balanced excitation and inhibition by active behavioral states in auditory cortex. *Nature Neurosci.* **17,** 841–850 (2014).
24. Bennett, C., Arroyo, S. & Hestrin, S. Subthreshold mechanisms underlying state-dependent modulation of visual responses. *Neuron* **80,** 350–357 (2013).
25. Niell, C. M. & Stryker, M. P. Modulation of visual responses by behavioral state in mouse visual cortex. *Neuron* **65,** 472–479 (2010).
26. Otazu, G. H., Tai, L. H., Yang, Y. & Zador, A. M. Engaging in an auditory task suppresses responses in auditory cortex. *Nature Neurosci.* **12,** 646–654 (2009).
27. Carmel, P. W. & Starr, A. Acoustic and nonacoustic factors modifying middle-ear muscle activity in waking cats. *J. Neurophysiol.* **26,** 598–616 (1963).
28. Tan, A. Y. & Wehr, M. Balanced tone-evoked synaptic excitation and inhibition in mouse auditory cortex. *Neuroscience* **163,** 1302–1315 (2009).
29. Jaramillo, S., Borges, K. & Zador, A. M. Auditory thalamus and auditory cortex are equally modulated by context during flexible categorization of sounds. *J. Neurosci.* **34,** 5291–5301 (2014).
30. Poulet, J. F., Fernandez, L. M., Crochet, S. & Petersen, C. C. Thalamic control of cortical states. *Nature Neurosci.* **15,** 370–372 (2012).
31. Korn, H., Faber, D. S., Burnod, Y. & Triller, A. Regulation of efficacy at central synapses. *J. Neurosci.* **4,** 125–130 (1984).
32. Thomson, A. M., Deuchars, J. & West, D. C. Large, deep layer pyramid-pyramid single axon EPSPs in slices of rat motor cortex display paired pulse and frequency-dependent depression, mediated presynaptically and self-facilitation, mediated postsynaptically. *J. Neurophysiol.* **70,** 2354–2369 (1993).
33. Guo, Z. V. *et al.* Flow of cortical activity underlying a tactile decision in mice. *Neuron* **81,** 179–194 (2014).
34. Chen, T. W. *et al.* Ultrasensitive fluorescent proteins for imaging neuronal activity. *Nature* **499,** 295–300 (2013).
35. Alexander, G. E., Newman, J. D. & Symmes, D. Convergence of prefrontal and acoustic inputs upon neurons in the superior temporal gyrus of the awake squirrel monkey. *Brain Res.* **116,** 334–338 (1976).
36. Hackett, T. A., Stepniewska, I. & Kaas, J. H. Prefrontal connections of the parabelt auditory cortex in macaque monkeys. *Brain Res.* **817,** 45–58 (1999).
37. Phillips-Silver, J. & Trainor, L. J. Feeling the beat: movement influences infant rhythm perception. *Science* **308,** 1430 (2005).
38. Fu, Y. *et al.* A cortical circuit for gain control by behavioral state. *Cell* **156,** 1139–1152 (2014).
39. Horváth, J. & Burgyan, A. No evidence for peripheral mechanism attenuating auditory ERPs to self-induced tones. *Psychophysiology* **50,** 563–569 (2013).
40. Froemke, R. C., Merzenich, M. M. & Schreiner, C. E. A synaptic memory trace for cortical receptive field plasticity. *Nature* **450,** 425–429 (2007).
41. Crapse, T. B. & Sommer, M. A. Corollary discharge across the animal kingdom. *Nature Rev. Neurosci.* **9,** 587–600 (2008).
42. Buran, B. N., von Trapp, G. & Sanes, D. H. Behaviorally gated reduction of spontaneous discharge can improve detection thresholds in auditory cortex. *J. Neurosci.* **34,** 4076–4081 (2014).
43. Langguth, B. *et al.* Altered motor cortex excitability in tinnitus patients: a hint at crossmodal plasticity. *Neurosci. Lett.* **380,** 326–329 (2005).
44. Heinks-Maldonado, T. H. *et al.* Relationship of imprecise corollary discharge in schizophrenia to auditory hallucinations. *Arch. Gen. Psychiatry* **64,** 286–296 (2007).

Acknowledgements We thank the members of the Mooney laboratory for discussions regarding experimental design and data analysis; S. Lisberger, F. Wang and S. Shea for their valuable comments on the manuscript; and M. Booze for technical support and animal husbandry. D.M.S. is a fellow of the Helen Hay Whitney Foundation; A.N. was supported by the Holland-Trice Graduate Fellowship in Brain Sciences; R.M. was supported by NIH grant NS079929.

Author Contributions D.M.S., A.N. and R.M. initiated the project and designed the experiments. D.M.S. performed electrophysiological, optogenetic, and pharmacological experiments in head-fixed mice. A.N. performed electrophysiological experiments in unrestrained mice, two-photon calcium imaging in head-fixed mice, immunohistochemistry, and imaging. D.M.S. and A.N. analysed the data. D.M.S., A.N. and R.M. prepared the manuscript.

Author Information Reprints and permissions information is available at www.nature.com/reprints. The authors declare no competing financial interests. Readers are welcome to comment on the online version of the paper. Correspondence and requests for materials should be addressed to R.M. (mooney@neuro.duke.edu).

METHODS

All experimental protocols were approved by Duke University Institutional Animal Care and Use Committee. Male and female wild-type (C57BL/6) and transgenic (VGAT–ChR2, PV-Cre, Ai14 and Ai27) mice were purchased from Jackson Laboratories and were subsequently housed and bred in an onsite vivarium. Viral vectors were acquired from University of Pennsylvania Vector Core.

Stereotaxic Injections. Mice aged 2–4 months were anaesthetized with isoflurane (1–2% in O_2) and placed in a stereotaxic holder (Leica). For expression of ChR2 in auditory thalamic or M2 axon terminals, a midline incision was made to expose the skull, and a craniotomy was made over the medial geniculate body or M2 ipsilateral to the eventual recording site in the auditory cortex. A pulled glass pipette backfilled with AAV.2/1.hSyn.ChR2.EYFP.WPRE (medial geniculate body of wild-type) or AAV.2/1.hSyn.H1.Cre.EGFP (M2 of Ai27) was lowered into the brain and positioned in the centre of the corresponding brain region. Approximately 300 nl of virus was pressure-injected into the brain over the course of 20 min. For M2 injections, this volume was split between two injection sites separated along the rostral–caudal axis by ~1 mm. For histological visualization of M2 projections to the auditory cortex, 50–100 nl of AAV.2/1.hSyn.EGFP.WPRE was pressure-injected into the centre of M2 over the course of 10 min. Animals were allowed to recover for 14 days following the injection. For infecting PV^+ neurons with ChR2, 150–250 nl of AAV.2/1.EF1a.DIO.ChR2.EYFP.WPRE was pressure-injected into the centre of auditory cortex of PV-Cre mice over the course of 10 min. For calcium imaging experiments, superficial and deep layers of M2 of Ai14 mice were injected with approximately 50 nl of AAV.2/1hSyn.GCaMP6s.WPRE. For visualizing $M2_{ACtx}$ neurons, auditory cortex was injected with 100–200 nl of CAV2-Cre (Universitat Autonoma de Barcelona, Unitat de Producció de Vectors), resulting in tdTomato expression in neurons expressing Cre recombinase.

Intracellular recording from unrestrained mice. Intracellular recordings were made from the auditory cortex of male wild-type mice (2–4 months of age) using a custom-built miniature-motorized microdrive based on previous designs[45,46]. The microdrive consisted of a chassis constructed through stereolithography (Agile Manufacturing, Inc.), which housed a motorized linear actuator (part no. 0206A001B +02/1 47:1-Y2825, Faulhaber) and a glass microelectrode, which rested in a cradle integrated in the chassis design. Two metal screws were threaded through the chassis wall along the axis of the actuator to stabilize and position the microelectrode. A miniaturized headstage constructed from a four-layer printed circuit board and surface-mounted components was mounted to the chassis. Signals and command current were acquired and sent using an intracellular amplifier (Axoclamp-2B, Axon Instruments) connected to the headstage via a flexible tether cable (Omnetics).

Mice were anaesthetized with isoflurane (1–2% in O_2) and placed in a stereotaxic holder (Leica). Body temperature was maintained at 37° C with an electrical heating pad. The scalp overlying the skull was removed, and the skull was cleaned with several washes of saline and povidone-iodine antiseptic (Betadine). A small metal pin was glued to the skull, which permitted animal restraint and head manipulation during electrode placement. The microdrive was positioned over the auditory cortex at a 10–15 degree angle relative to vertical to facilitate electrode travel along the axis of auditory cortex. The base of the chassis was cemented to the skull with dental acrylic. A craniotomy was made over the contralateral somatosensory cortex and a silver chloride reference ground was rested on the brain, followed by bone wax and dental acrylic. Mice were given topical analgesic and supplementary feed, and were allowed to recover for at least three days.

On the first day of recording, animals were anaesthetized with isoflurane and restrained in a stereotaxic device. A small craniotomy (typically 100 × 100 μm) was made over the auditory cortex, and the dura was carefully resected with an insect pin. The exposed brain surface was coated with silicon oil (1000cs, Dow Corning). Sharp borosilicate glass electrodes were fabricated with a horizontal puller (P-97, Sutter Instruments), and tips were filled with 3 M K-acetate containing 5% neurobiotin. Electrodes were cut to size and backfilled with 3 M K-acetate, resulting in electrode impedances ranging from 80 to 120 MΩ. An electrode was attached to a metal shuttle, which travelled along the linear actuator. A copper fabric Faraday cage connected to an electrical ground then covered the entire assemblage to limit both electrical and mechanical interference. The mouse was released from restraint and allowed to fully recover for at least 30 min before recordings were made. The electrode was advanced in the brain until the tip penetrated a neuron. Intracellular signals were acquired with a Power 1401 using Spike 2 (Cambridge Electronic Design), and used for further analysis only if the resting membrane potential was less than −50 mV and was modulated by an auditory stimulus. At the end of a recording session, the electrode was removed and the brain surface was coated with silicon elastomer (Kwik-Cast, WPI) until the following recording session. Vocalizations were elicited by presenting a cotton swab with 20 μl of urine from female mice. Data collected from unrestrained mice are included in analyses of movement-related changes in membrane potential dynamics (Fig. 1c, e), movement-related changes in excitability (Fig. 2h), and membrane potential changes during vocalization (Extended Data Fig. 2a, b, g).

Intracellular recording from head-restrained mice. One to three days before physiology, mice were anaesthetized with isoflurane and a custom plate that left auditory cortex and frontal cortex exposed was attached to the skull with cyanoacrylate and Meta-bond (Parkell). Ink dots were placed on the surface of the skull at stereotaxic coordinates over the auditory cortex and M2. On the day of physiology, mice were positioned on top of a 7-inch Styrofoam cylinder[47] or at the periphery of a 7-inch spinning disk (Flying Saucer, Foster and Smith), held in place by two clamps (Standa). In both preparations, mice freely transitioned between periods of rest and movement. Mice were briefly anaesthetized with isoflurane and a small craniotomy was made over the auditory cortex. A sharp electrode was placed in an Axoclamp headstage (HS-2A) and was lowered vertically into the brain with a hydraulic manipulator (SD Instruments) until the tip penetrated a neuron. Intracellular signals were acquired and processed as in unrestrained experiments. Tone presentation and laser stimulation were controlled with custom software (Spike2, CED). A small video camera (Logitech) was positioned to monitor treadmill and body movements, and an optical mouse was positioned near the treadmill to monitor its rotational velocity in real time. An ultrasonic-sensitive microphone (Avisoft Bioacoustics) was also positioned near the mouse to monitor sounds. Video, treadmill rotation and physiology recordings were synchronized post hoc based on an aperiodic train of digital pulses (mean rate: ~0.2 Hz) that was simultaneously sent to all acquisition devices. For pharmacologically silencing M2, a craniotomy was made that spanned ~2.5 mm along the rostral-caudal axis of M2, the dura was removed, and 20 μM TTX was applied to the brain surface. Neural activity in M2 was monitored before, during and after TTX administration with an extracellular array spanning all cortical layers and positioned at the rostral and caudal ends of the craniotomy to ensure suppression of spontaneous and antidromic activity.

Extracellular recording from head-restrained mice. Surgical, behavioural, data recording and stimulus presentation were the same as intracellular recordings in head-fixed mice. A 32-channel (4 × 8; 0.8 × 0.8 mm recording area) multi-electrode array (NeuroNexus) was lowered vertically into either M2 or the auditory cortex and allowed to rest for 30 min. The electrode array was connected directly to a digitizing headstage (Intan Technologies) via a 36-pin connector (Omnetics). Neural activity was referenced to an Ag-Cl pellet implanted over contralateral somatosensory cortex. Analogue traces were filtered (300 to 5,000 Hz), digitized, and recorded (20 kHz per channel) for offline analysis. Putative action potentials were identified based on deviation from the mean and individual neurons were sorted based on spike features (WaveClus[48]). Recordings were coupled with blue light stimulation over the brain surface, directed towards the recording face of the electrode array. Identified PV^+ interneurons were excited by blue light in PV–ChR2 mice and always had fast action potentials. Identified inhibitory interneurons were excited by blue light in VGAT–ChR2 mice and typically had fast action potentials. Putative excitatory neurons had broad action potentials and were suppressed by blue light stimulation in VGAT–ChR2 mice.

Calcium imaging. Two weeks following the GCaMP6s injection, mice were anaesthetized with isoflurane and a custom, horse-shoe-shaped plate was attached to the skull with cyanoacrylate and Meta-bond (Parkell). Mice were acclimated to head fixation for 1–3 days before the initial imaging session, and 30 μl dexamethasone (4 mg ml^{-1}) was administered (intramuscularly) on the last acclimation day, 6–12 h before windowing. A rectangular craniotomy was then made over the injection site, and a laminated glass coverslip assemblage was placed over the craniotomy and sealed with Meta-bond. Mice were allowed to recover and imaging proceeded in a room illuminated only with infrared light. Imaging was performed using a two-photon microscope (Zeiss LSM 510) with a mode-locked titanium sapphire laser at 910 nm. Images were acquired at up to 10 Hz with a ×40 water-immersion objective while the mouse volitionally transitioned between periods of rest and movement. A small infrared-sensitive video camera (Logitech) was positioned to monitor treadmill and body movements. Video and acquired images were synchronized post hoc based on an aperiodic train of digital pulses (mean rate: ~0.2 Hz) that was simultaneously sent to all acquisition devices. Images were registered using the ImageJ plugin TurboReg to correct for movement artefact in the horizontal plane. ROIs were selected manually using average intensity projections of image time-series, and $\Delta F/F$ for each ROI was calculated in Matlab with user-defined periods of basal fluorescence. $\Delta F/F$ traces were aligned and averaged within cell with respect to movement onset, determined as described below.

Optogenetic stimulation in head-restrained mice. For stimulation over the auditory cortex, the skull was thinned lateral to the physiology craniotomy and a fibre optic cable was positioned over the thinning at a 0–30 degree angle relative to horizontal, directed towards the location of the recording electrode. For stimulation over M2, the skull was thinned or removed over M2 and a fibre optic cable was positioned over the brain at a 60–90 degree angle relative to horizontal, directed down and towards the midline. The junction between the fibre and the skull or brain was coated in silicon

oil, and the other end of the fibre was coupled to a blue laser (473 nm, Shanghai). For stimulation of M2 cell bodies or M2 terminals in the auditory cortex, laser illumination was controlled manually for variable durations (0.2 to 2.0 s) or was automated to deliver fixed-duration pulses with a constant inter-pulse interval. For stimulation of thalamic terminals, brief (5 ms) pulses of light were delivered with an inter-pulse interval of ~4 s. For paired-pulse stimulation of thalamic terminals in the auditory cortex, two brief (5 ms) pulses of light were separated by 50 ms, repeated every 4 s. Laser power ranged from 4 mW mm^{-2} to 32 mW mm^{-2}.

Behavioural analysis. An optical treadmill monitor was constructed by positioning the optics of a disassembled computer mouse near the treadmill. The USB end of the optical mouse was plugged into a data acquisition card (Arduino Mega) that was programmed to monitor treadmill displacement (custom software adapted from ref. 49), which was sampled at ~100 Hz using custom software (Matlab). Rotational velocity was calculated by determining the number of pixels that corresponded to one rotation of the treadmill and through post hoc calibration with simultaneous video recordings.

Videos were analysed offline to detect treadmill, forelimb, body, and facial movements during head-fixed experiments, and to detect head movements, body movements and translocation in unrestrained experiments. Two-dimensional regions of interest (ROIs) were defined for the contralateral forelimb, torso, face (including mouth, nose and whiskers), and treadmill, as well as for a red LED that was used to synchronize video and physiology data. Within each ROI, the average change in pixel intensity was calculated across subsequent frames (30 Hz sampling rate) as a measure of movement. For unrestrained experiments, a single ROI encompassed the entire arena and movements included either gross changes in posture that resulted in body movement greater than 10 mm or translocation of distances greater than 2.5 cm that lasted for at least 1 s.

Histology and imaging. Mice were deeply anaesthetized with sodium pentobarbital (250 mg per kg, intraperitoneally) and transcardially perfused with phosphate buffered saline (PBS) followed by 4% cold paraformaldehyde. Brains were post-fixed overnight in 4% paraformaldehyde containing 30% sucrose. Brains were blocked in Optimum Cutting Temperature compound (Tissue-Tek), and 50-μm coronal sections were cut on a sliding freezing microtome. Brain slices were first rinsed in PBS for 10 min, then in two washes of PBS containing 0.3% Triton X-100 (PBST) for 20 min. Slices were then incubated in PBST with 10% Blocking One blocking buffer (Nacalai Tesque) for 1 h at room temperature. Immunostaining was performed with primary antibodies of rabbit anti-GFP (1:1,000; Abcam), mouse anti-parvalbumin (1:1,000; Swant), or mouse anti-NeuN (1:100, Millipore) in PBST containing 10% blocking buffer for three days at 4 °C. After three washes of 10 min in PBS, slices were incubated in secondary antibodies from Jackson Immunoresearch at a concentration of 1:1000 in PBST containing 10% blocking buffer overnight at 4 °C. Sections were washed several times in PBS, incubated in PBS containing DAPI for 30 min, rinsed again, and mounted. For visualizing neurobiotin cell fills, permeabilized 75 μm sections were incubated overnight in PBST containing streptavidin Alexa 546 or Alexa 488. All images were acquired with a Zeiss 710 LSM confocal microscope.

Statistical analyses. All distributions passed tests for normality (Kolmogorov–Smirnov). Student's *t*-test, paired *t*-test and Two-sampled *t*-test were used as described below. Sample sizes were chosen to ensure adequate power with the statistical tests used. For all statistical tests, significance was measured against alpha of 0.05. Randomization was not used to determine how animals were allocated to experimental groups, nor were investigators blinded to group allocation. Automated calculation of membrane potential mean and variance, tone-evoked responses, and movement onset/offset allowed the investigator to be blind to movement/rest and laser ± conditions. Statistical details for experiments described in Figs 1–5 are detailed below, including the sample size (number of neurons and number of mice), population mean ± s.d. values, exact *P* values and statistical tests.

Figure 1e. For comparing membrane potential variance and mean measured during periods of rest vs movement, data were analysed separately for microdrive and treadmill recordings. Microdrive: $n = 16$ cells from 9 mice; V_m variance was 12.58 ± 10.48 mV during rest and 4.22 ± 2.69 mV during movement ($P = 0.0009$, paired *t*-test). V_m mean was −91.62 ± 17.23 mV during rest and −87.62 ± 16.31 mV during movement ($P = 6 \times 10^{-5}$, paired *t*-test). Treadmill: $n = 37$ cells from 11 mice; V_m variance was 10.7 ± 8.5 mV during rest and 4.6 ± 3.3 mV during movement (P = 8e-7, paired *t*-test); V_m mean was −85.2 ± 15.3 mV during rest and −81.4 ± 14.3 mV during movement ($P = 1 \times 10^{-5}$, paired *t*-test).

Figure 1g. Changes in membrane potential mean relative to movement onset and offset were calculated from data collected with the treadmill preparation ($n = 25$ cells from 7 mice). Time of V_m change relative to movement onset was −225 ± 573 ms ($P = 0.06$, *t*-test). Time of V_m change relative to movement offset was 271 ± 383 ms ($P = 0.01$, *t*-test).

Figure 2b. Change in tone-evoked response during movement vs rest was calculated from data collected with the treadmill preparation ($n = 27$ cells from 6 mice). Voltage area was 8.67 ± 4.39 mV s during rest and 2.97 ± 3.68 mV s during movement ($P = 8 \times 10^{-9}$, paired *t*-test).

Figure 2e. Change in tone-evoked response ($n = 27$ cells from 6 mice) and thalamic terminal stimulation response ($n = 9$ cells from 2 mice) were calculated from data collected with the treadmill preparation. The peak tone or stimulation response (in mV) during movement was normalized by the peak response during rest. For tone presentation, the peak response during movement was 0.54 ± 0.22 relative to rest ($P = 4 \times 10^{-13}$, *t*-test). For terminal stimulation, the peak response during movement was 0.72 ± 0.21 relative to rest ($P = 0.0005$, *t*-test).

Figure 2h. Excitability was measured by counting the number of spikes evoked by a periodic injection of depolarizing current through the recording electrode during rest and movement. Data include 5 cells from 5 mice using the microdrive and 5 cells from 3 mice using the treadmill. Spike counts were 5.25 ± 2.34 during rest and 1.08 ± 1.04 during movement ($P = 0.0005$, paired *t*-test).

Figure 2j. Input resistance was measured by calculating the change in V_m during hyperpolarizing current injection divided by the amount of current injected. Data include 10 cells from 5 mice using the treadmill. Input resistance was 35.9 ± 8.9 MΩ during rest and 28.0 ± 11.1 MΩ during movement ($P = 0.0007$, paired *t*-test).

Figure 2l. EPSP slope was measured by calculating the change in V_m during the initial rising phase of the EPSP (~2 ms), which was primarily linear. For paired-pulse experiments, the slope of the EPSP in response to the second pulse was normalized by the slope of the EPSP in response to the first pulse ($n = 7$ cells from 1 mouse using treadmill, 0.53 ± 0.25, $P = 0.002$, *t*-test). For movement vs rest, the slope of the EPSP measured during movement was normalized by the slope of the EPSP measured during rest ($n = 9$ cells from 4 mice using treadmill, 0.95 ± 0.21, $P > 0.1$, *t*-test).

Figure 3c. Extracellular recordings were made from identified excitatory neurons (black, $n = 173$ cells from 5 mice) and PV$^+$ inhibitory neurons (green, $n = 12$ cells from 2 mice) in the auditory cortex, and from identified excitatory neurons in M2 (blue, $n = 90$ cells from 3 mice). Significance thresholds were determined by calculating the 95th percentile of baseline firing rates for each population independently.

Figure 3f. Calcium transients were obtained from identified M2$_{ACtx}$ neurons (tdTomato$^+$, $n = 7$ cells from 2 mice) and unlabelled M2 neurons (tdTomato$^-$, $n = 23$ cells from 2 mice).

Figure 4e. V_m variance without silencing M2 cell bodies was 6.4 ± 4.4 mV during rest and 2.7 ± 2.0 mV during rest+laser ($n = 15$ cells from 4 mice, $P = 0.003$, paired *t*-test). V_m variance with M2 cell bodies silenced was 7.6 ± 8.8 mV during rest+TTX and 2.4 ± 1.9 mV during rest+TTX+laser ($n = 14$ cells from 2 mice, $P = 0.02$, paired *t*-test).

Figure 4f. V_m mean without silencing M2 cell bodies was 2.3 ± 3.3 mV during rest+laser, relative to rest ($n = 15$ cells from 4 mice, $P = 0.016$, *t*-test). V_m mean with M2 cell bodies silenced was 1.7 ± 2.0 mV during rest+TTX+laser, relative to rest+TTX ($n = 14$ cells from 2 mice, $P = 0.009$, *t*-test).

Figure 4g. Peak tone response without silencing M2 cell bodies was 6.2 ± 3.2 mV during rest and 4.1 ± 1.7 mV during rest+laser ($n = 13$ cells from 4 mice, $P = 0.008$, paired *t*-test). Peak tone response with M2 cell bodies silenced was 8.4 ± 4.7 mV during rest+TTX and 5.6 ± 4.2 mV during rest+TTX+laser ($n = 9$ cells from 2 mice, $P = 0.01$, paired *t*-test).

Figure 4h. The latency to changes in V_m mean after M2 terminal stimulation was calculated with (red, $n = 15$ cells from 4 mice) and without (black, $n = 14$ cells from 2 mice) M2 cell bodies inactivated with TTX. Significance thresholds were determined by calculating the 95th percentile of baseline V_m for each population independently.

Figure 5f. Silencing of ipsilateral and contralateral M2 in VGAT–ChR2 mice was reproduced multiple times while recording from a subset of neurons. Distributions represent 27 experiments from 10 cells from 6 mice for ipsilateral silencing and 12 experiments from 5 cells from 2 mice for contralateral silencing.

Figure 5g. V_m variance was 5.0 ± 2.3 mV during rest, 5.5 ± 2.9 mV during rest+laser, 2.1 ± 0.7 mV during mvmt, and 5.7 ± 2.8 mV during mvmt+laser ($n = 10$ cells from 6 mice; rest vs mvmt, $P = 0.0006$; mvmt vs mvmt+laser, $P = 0.0007$; paired *t*-test for all comparisons).

Figure 5h. V_m mean relative to resting condition was -0.01 ± 3.4 mV during rest+laser, 3.4 ± 2.5 mV during mvmt, and 1.0 ± 2.3 mV during mvmt+laser ($n = 10$ cells from 6 mice; rest vs mvmt, $P = 0.002$; mvmt vs mvmt+laser; $P = 0.0009$; paired *t*-test for all comparisons).

Figure 5j. Peak tone-evoked responses were measured during rest and movement, with and without optogenetically silencing ipsilateral M2, and were normalized to the rest condition. Peak tone response relative to rest was 1.1 ± 0.05 during rest+laser, 0.43 ± 0.20 during mvmt, and 0.65 ± 0.14 during mvmt+laser ($n = 7$ cells from 2 mice; rest vs rest+laser, $P = 0.024$; rest vs mvmt, $P = 0.0002$; mvmt vs mvmt+laser, $P = 0.002$; paired *t*-test for all comparisons).

Figure 5g, j. We ran a two-factor ANOVA with repeated measures to determine whether there was a significant interaction between laser stimulation and movement on auditory cortical dynamics when optogenetically silencing M2 in VGAT–ChR2

mice. Movement (+/−) and laser stimulation (+/−) were independent variables and membrane potential variability (Fig. 5g) or peak tone response (Fig. 5j) were dependent variables. Both analyses revealed significant interaction terms ($P < 0.05$).

45. Hamaguchi, K., Tschida, K. A., Yoon, I., Donald, B. R. & Mooney, R. Auditory synapses to song premotor neurons are gated off during vocalization in zebra finches. *eLife* **3,** e01833 (2014).
46. Long, M. A., Jin, D. Z. & Fee, M. S. Support for a synaptic chain model of neuronal sequence generation. *Nature* **468,** 394–399 (2010).
47. Wienisch, M., Blauvelt, D. G., Sato, T. F. & Murthy, V. N. Two-photon imaging of neural activity in awake, head-restrained mice. *Neuromethods* **67,** 45–60 (2012).
48. Quiroga, R. Q., Nadasdy, Z. & Ben-Shaul, Y. Unsupervised spike detection and sorting with wavelets and superparamagnetic clustering. *Neural Comput.* **16,** 1661–1687 (2004).
49. Sanders, J. I. & Kepecs, A. Choice ball: a response interface for two-choice psychometric discrimination in head-fixed mice. *J. Neurophysiol.* **108,** 3416–3423 (2012).

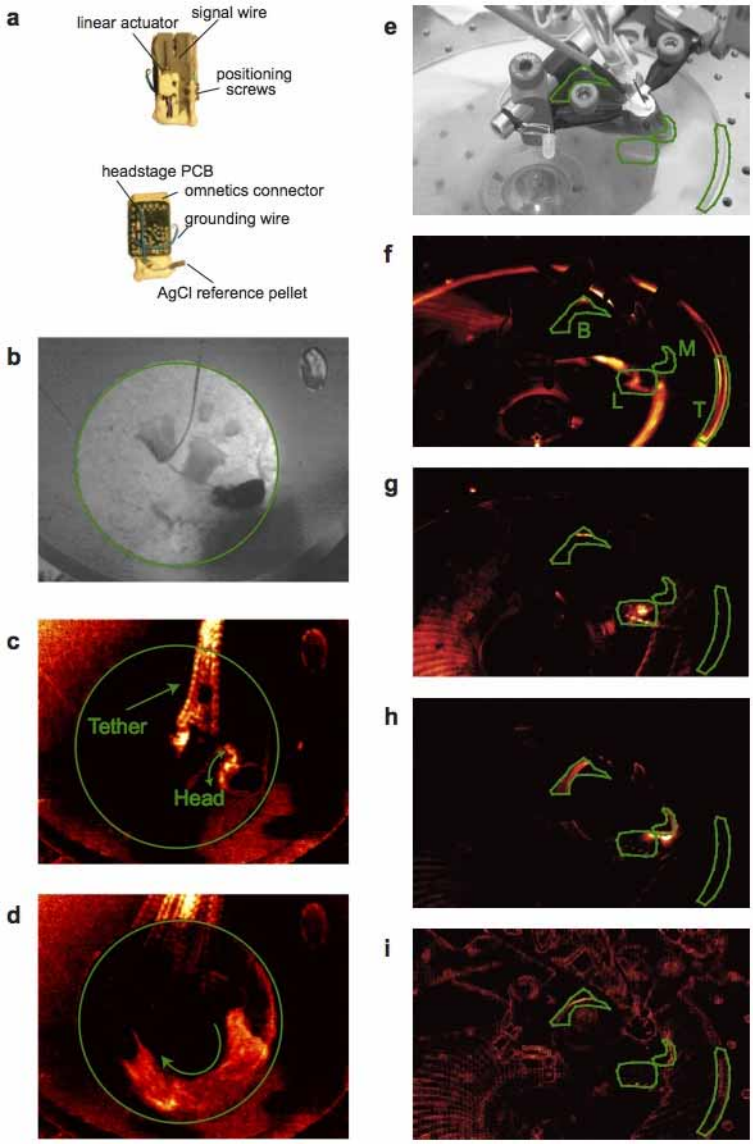

Extended Data Figure 1 | Analysis of behaviour in unrestrained and head-fixed mice. **a**, The miniature-motorized microdrive used for making intracellular recordings from unrestrained mice. **b**, Video still of unrestrained mouse in a circular arena during microdrive recording. Green circle indicates full-field ROI that was used for semi-automated movement detection. **c**, Changes in pixel intensity over time were measured to detect movements and the heat map shows the average change in pixel intensity across frames for a 2-s clip. Image in **c** shows a back-and-forth head movement as indicated by green arrows. **d**, As in **c**, but for translocation in the direction indicated by the green arrow. **e**, Video still of head-restrained mouse positioned on a circular treadmill. Green polygons show regions of interest for the treadmill (T), body (B), forelimb (L) and facial (M), with labels shown in **f**. **f**–**i**, Heat maps showing average movement for 2-s video clips during running (**f**), forelimb movements (**g**), grooming (**h**) and facial movements (**i**).

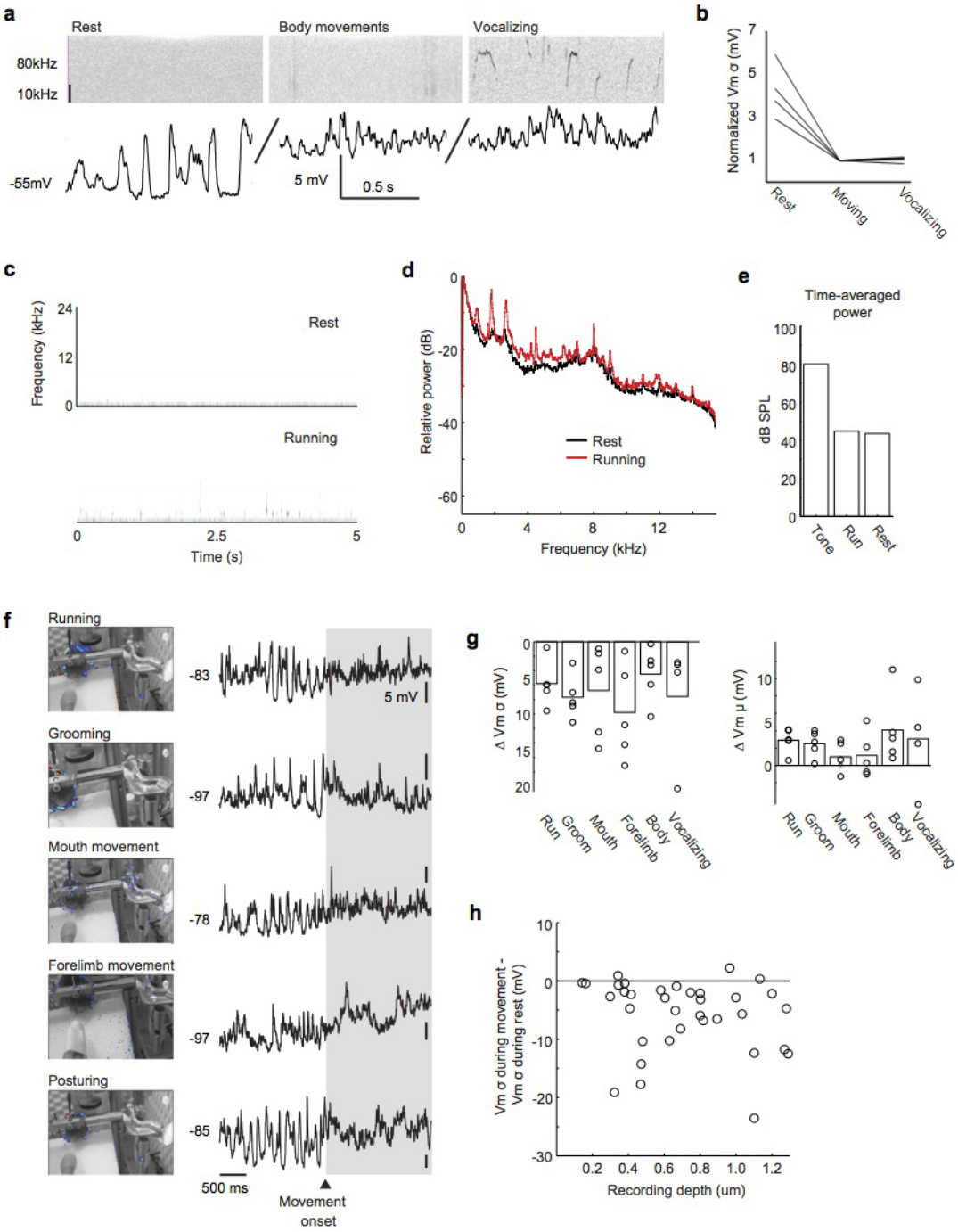

Extended Data Figure 2 | Motor-related dynamics across a variety of behaviours. **a**, Top shows spectrogram of sound recorded during microdrive experiment, bottom is simultaneous current-clamp recording from auditory cortical excitatory neuron. Left panel shows rest, middle panel shows movement, and right panel shows vocalization ($n = 5$ cells from 3 mice; moving versus moving and vocalizing, $P = 0.3733$, paired t-test). **b**, Normalized membrane potential variance during rest, body movements, and vocalizations. **c**, Spectrograms of head-fixed mouse on treadmill during 5-s periods of rest (top) and running (bottom). **d**, Power spectra of sound measured during rest and running. The power spectra are indistinguishable at frequencies greater than 12 kHz. **e**, Mean root mean square (RMS) power (in dB sound pressure level (SPL)) of tone playback (80 dB), running (43 dB) and rest (42 dB). **f**, Left panels show static images of head-fixed mouse with heat maps indicating regions of movement during the movement epochs shown at right. Right panels show current-clamp recordings during the movements depicted on the left. **g**, Change in membrane potential variance (left) and mean (right) for 5 examples of unique movements and 4 examples of vocalization ($n = 5$ cells from 5 mice for non-vocalizing movements). **h**, Change in variance as a function of recording depth.

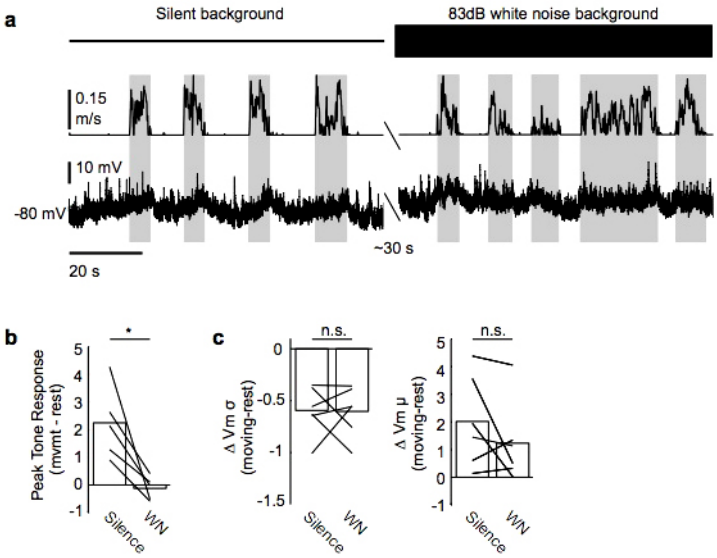

Extended Data Figure 3 | Motor-related dynamics persist in broadband masking noise. **a**, Example neuron recorded during movement and rest and during periods of silence (left) and 83 dB white noise playback (right). Top panel shows ambient environment, middle panel shows treadmill velocity, and bottom panel shows membrane potential. **b**, White noise masking abolishes tone-evoked responses ($n = 5$ cells from 2 mice, $P < 0.05$, paired t-test). **c**, Masking does not alter changes in membrane potential variance or mean exhibited during movement ($n = 6$ cells from 2 mice).

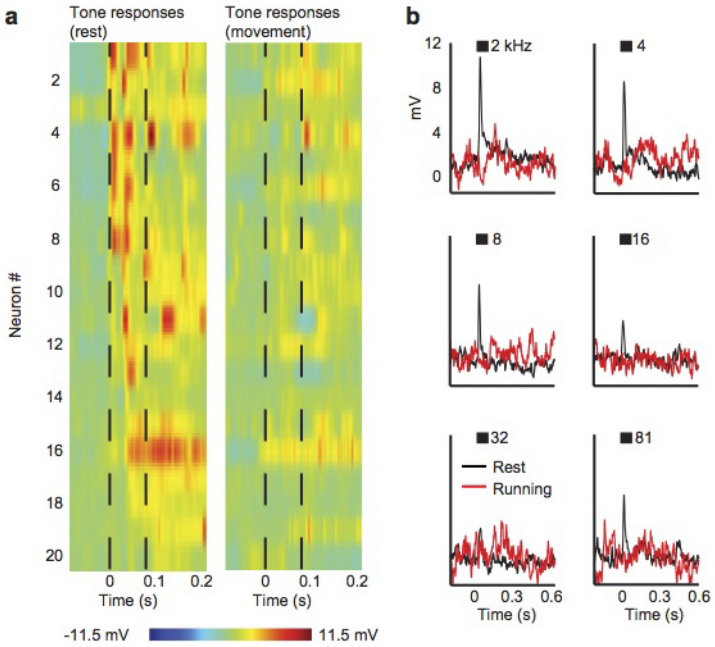

Extended Data Figure 4 | Tone-evoked responses are suppressed during movement. **a**, Tone-evoked synaptic responses from 20 auditory cortical excitatory neurons during rest (left) and during movement (right). Black dashed lines show tone onset and offset. The tone presented to each neuron was chosen to evoke the largest response ($n = 20$ cells from 6 mice). **b**, Mean synaptic responses from a single neuron to multiple presentations of tones presented at multiple frequencies. Black shows response during rest, red shows response during movement. Black bars indicate duration of tone.

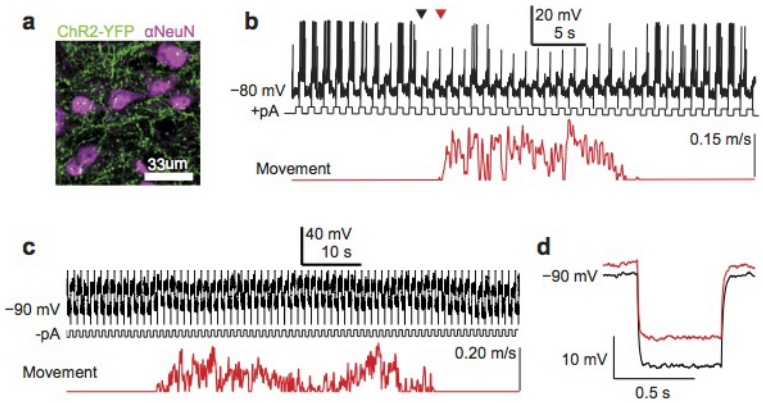

Extended Data Figure 5 | Excitability and input resistance decrease during movement. **a**, Confocal micrograph of ChR2^{+} thalamocortical terminals (green) amidst neurons immunostained for NeuN (magenta). **b**, Top panel shows spiking response of an auditory cortical excitatory neuron recorded in treadmill preparation to positive current pulses injected with the recording electrode. Bottom trace shows treadmill movement. The onset of motor-related changes in excitability (black triangle) precedes movement onset (red triangle). **c**, Top panel shows membrane potential response of an auditory cortical excitatory neuron to negative current pulses injected with the recording pipette. Bottom trace shows treadmill movement. **d**, Average hyperpolarizing response to negative current pulses injected during rest (black) and during movement (red).

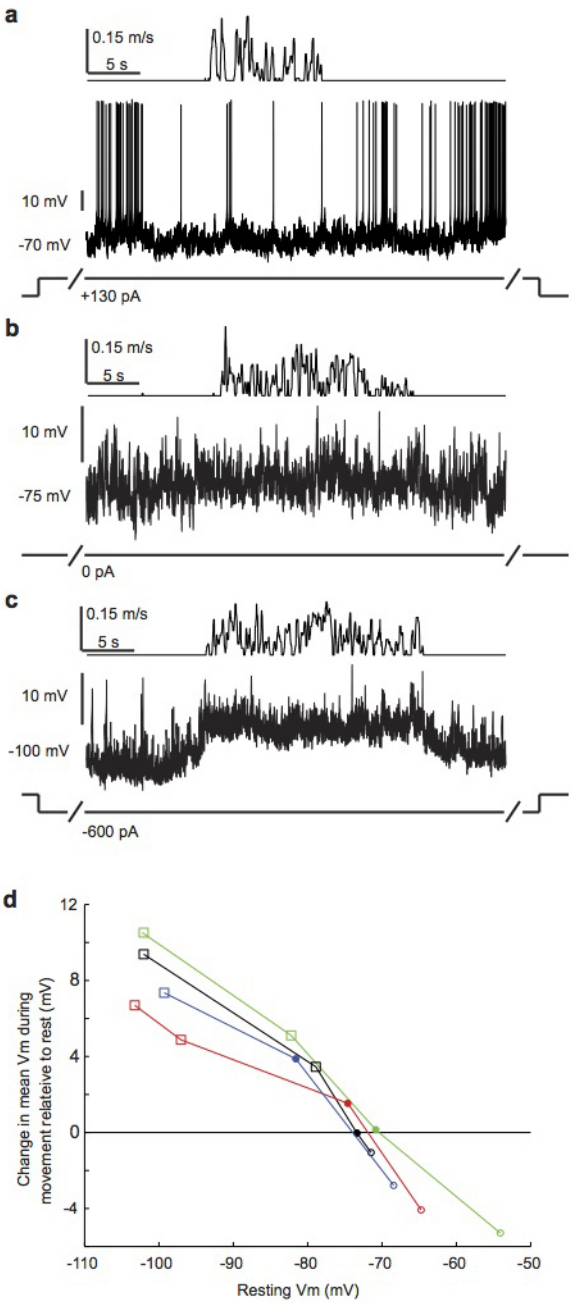

Extended Data Figure 6 | Estimating the reversal potential of motor-related currents. **a**, Auditory cortical excitatory neuron recorded with treadmill preparation as mouse transitions from rest to movement and back to rest. Top panel shows treadmill movement. Prior to and throughout movement, neuron was depolarized with positive current injection with recording pipette. **b**, Same neuron as **a**, but with no current injection. **c**, Same neuron as **a**, but with hyperpolarizing current injection. **d**, Change in mean membrane potential during movement relative to rest as a function of the membrane potential before movement for 4 neurons from 4 mice. Filled circles indicate movements without current injection. Open circles show movements with depolarizing current injection. Open squares show movements with hyperpolarizing current injection. Movement-related modulation of mean membrane potential switches from depolarizing to hyperpolarizing when the resting membrane potential exceeds approximately −72 mV.

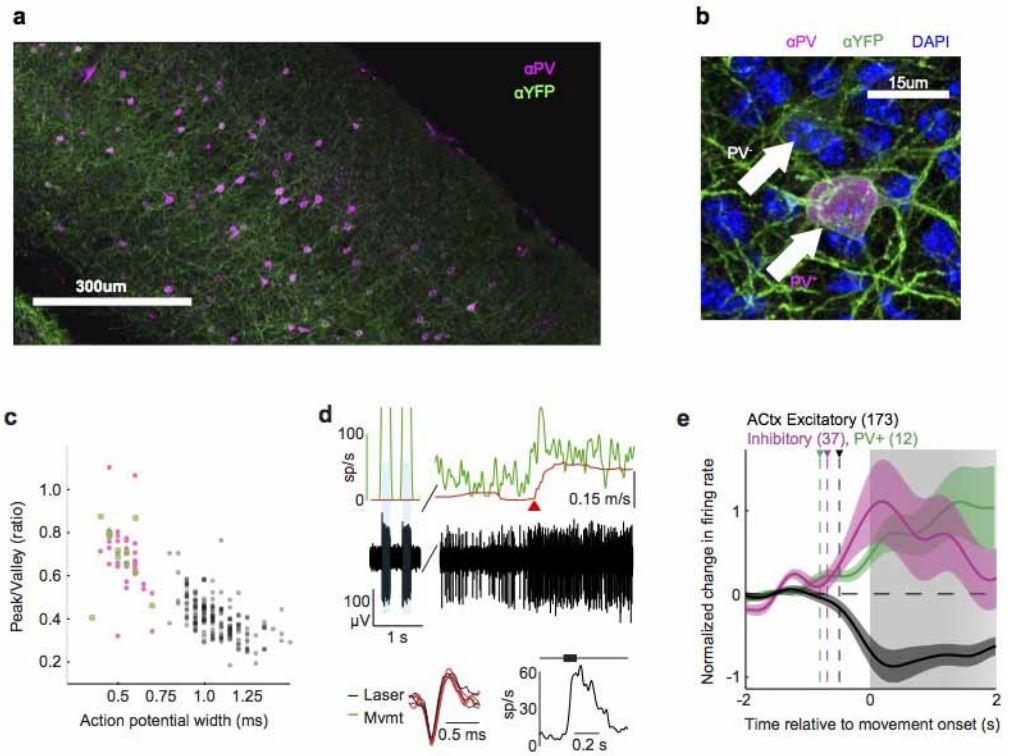

Extended Data Figure 7 | Inhibitory activity increases during movement. **a**, Composite micrograph of a coronal slice of auditory cortex from a VGAT–ChR2–YFP mouse, immunostained for YFP (yellow fluorescent protein; green) and parvalbumin (PV, magenta). **b**, High magnification image of a section from **a**, showing both PV^+ (magenta) and PV^- interneurons expressing ChR2 (green). **c**, Scatter plot showing action potential width and peak-to-valley ratio for all identified PV^+ interneurons (green), identified $VGAT^+$ interneurons (magenta), and putative excitatory neurons (grey) in the auditory cortex. **d**, Identified PV^+ interneuron recorded from PV–ChR2 mouse. Top panel shows treadmill velocity (red), instantaneous firing rate (green) and raw voltage trace (black) recorded during laser stimulation (blue shaded regions), rest and locomotion. Instantaneous firing rate during laser stimulation was truncated and reaches a maximum of 500 spikes per s. Red triangle indicates time of movement onset. Bottom left shows overlaid action potential waveforms produced during laser stimulation (black, $n = 3$) and locomotion (red, $n = 3$). Bottom right shows average sound-evoked response to tone presented at neuron's preferred frequency. **e**. Normalized change in firing rate aligned to movement onset for PV^+ neurons (green, described in main figure), $VGAT^+$ interneurons (pink, $n = 37$ cells from 3 mice) and putative excitatory neurons (grey, described in main figure).

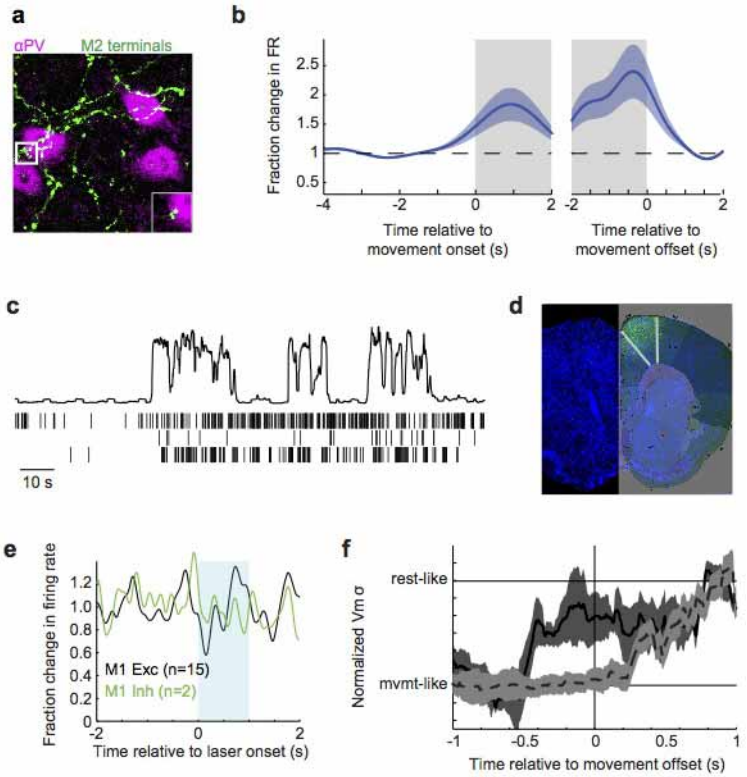

Extended Data Figure 8 | M2 activity drives motor-related changes in auditory cortical dynamics. **a**, *Z*-stack micrograph of M2 axons (green, AAV-GFP injection) forming appositions with PV^+ immunostained interneurons in auditory cortex (magenta). Inset shows a high magnification single (2 μm) optical section of an apposition. **b**, M2 spiking activity relative to movement onset (left) and offset (right), normalized to pre-movement activity ($n = 90$ cells from 3 mice). **c**, Three simultaneously recorded M2 neurons during three transitions from rest to movement. Top panel shows movement extracted from video (arbitrary units, a.u.). **d**, Cell bodies and local terminal field of $ChR2^+$ neurons following injection of AAV.2/1.ChR2 into M2. Image is overlaid with an atlas from the Allen Brain Institute. **e**, Extracellular recordings in M1 of VGAT–ChR2 mouse during blue laser stimulation over ipsilateral M2 showing no change in firing of neurons with broad (black, putative excitatory) or narrow (green, putative inhibitory) neurons ($n = 17$ cells from 1 mouse). **f**, Change in membrane potential variance of auditory cortical excitatory neurons over time during optogenetic silencing of either ipsilateral (black, solid, $n = 10$ cells from 6 mice) or contralateral (grey, dashed, $n = 5$ cells from 2 mice) M2. For each neuron, the time-varying membrane potential variance was measured during a sliding window that extended 500 ms into the past. Traces were then averaged across neurons after aligning each to the time of movement cessation. Silencing ipsilateral M2 causes membrane potential variance to change before movement offset, whereas silencing contralateral M2 causes the variance to change after movement offset.